Nanoscale Morphology Control Using Ion Beams

M.J. Aziz

Division of Engineering and Applied Sciences
Harvard University
Cambridge, MA 02138, U.S.A.

Abstract

Ion irradiation of a solid surface can be used to control surface morphology on length scales from 1 micron to 1 nanometer. Focused or unfocused ion irradiation induces a spontaneous self-organization of the surface into nanometer-sized ripples, dots, or holes; it also induces diameter increases and decreases in pre-existing nanopores. The phenomenology of the surface morphological evolution under ion beam erosion is reviewed with an emphasis on semiconducting materials, including recent experiments on the influence of boundary conditions on guiding self-organized pattern formation; the development of shock fronts that sharpen features at sufficiently steep angles; and the kinetics governing the fabrication of nanopores for single-biomolecule detectors. The theory underlying the surface morphology evolution is reviewed and areas of agreement and disagreement with experiment are identified.

Contents

1. Introduction

Nanoscale surface morphologies spontaneously develop from uniform ion irradiation of an initially flat surface in a non-equilibrium self-organization process termed "sputter patterning". Spontaneous self-organization processes such as this have no fundamental throughput limitations and have been used to create patterns with lateral feature sizes as small as 15 nm, and good short-range order (Facsko et al., 1999) as shown in Figure 1. As in most self-organization processes, the major challenge is the flexibility one has over the resulting pattern. A combination of "top-down" approaches for flexibility and "bottom-up" approaches for size and throughput is likely to be a successful strategy for mass production of functional nanoscale devices. The importance of the "bottom-up" approaches will be determined to a significant degree by the answer to the question, "how much control do we have over the morphology?" A great deal of fundamental research must be done before this question can be answered.

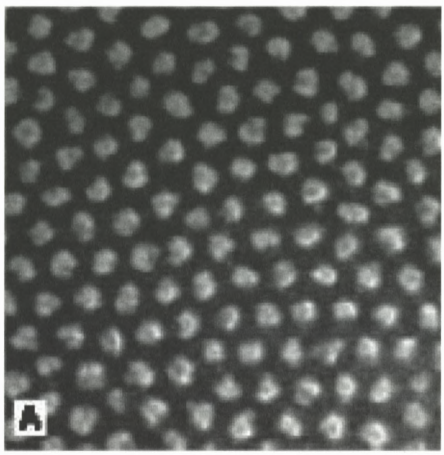

Figure 1. "Quantum dots" on GaSb, fabricated by normal-incidence sputter patterning using 420 eV Ar^+. From Facsko et al. (1999). Image 500 nm × 500 nm. Dots as small as 15 nm have been reported.

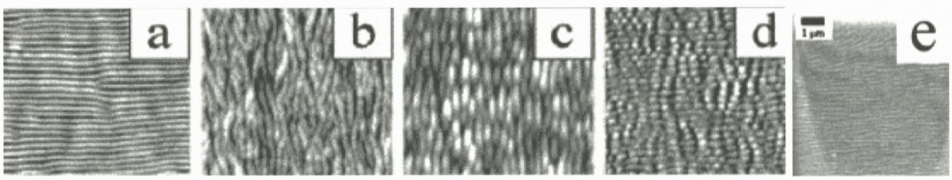

Figure 2. Sputter patterns formed on Si. (a) highly aligned "parallel mode" ripples on Si(111), from Brown et al. (2005), (b) wavy "perpendicular mode" ripples on Si(001) (Erlebacher et al., 1999), (c) wavy perpendicular mode ripples on Si(111), from Brown et al. (Brown et al., 2005), (d) two dimensional dot arrays on Si(111), from Brown et al. (Brown et al., 2005), (e) ripples in *a*-Si formed by uniform FIB rastering (Cuenat and Aziz, 2002). Projected ion beam direction is from bottom to top in all images. AFM scan size for (a)–(d) is 10 microns. Scale bar in SEM image in (e) is 1 micron.

In a related phenomenon, ion irradiation permits nanopore morphology control on the single-digit nanometer level and is consequently termed "ion beam nano sculpting". Solid state nanopores with diameters of molecular dimensions have been fabricated this manner (Li et al., 2001). The technology is being used to make single biomolecule detectors that are now capable of analyzing biomolecule lengths and molecular conformations in vitro and are envisaged as ultra-rapid DNA sequencers.

In this paper we discuss the scientific aspects of ion-solid interactions underlying these developments.

2. Sputter Patterning

2.1. Formation of Sputter Patterns

It has long been known that under some conditions of uniform ion irradiation of a solid surface, a spontaneously-arising sputter pattern topography arises that often takes the form of one-dimensional ripples or two-dimensional arrays of dots. The periodicity is understood to arise as a result of a kinetic competition between the surface roughening effect of the ion beam and morphological relaxation.

There is a significant body of experimental and theoretical work on ion-stimulated formation and relaxation of self-organized topographic features on solid surfaces (Navez et al., 1962; Bradley and Harper, 1988; Erlebacher and Aziz, 1997; Habenicht, 2001; Makeev et al., 2002; Valbusa et al., 2003; Brown and Erlebacher, 2005). Figure 2 shows representative surface morphologies on Si, including regular and irregular one-dimensional ripples formed at off-normal ion beam incidence (Erlebacher et al., 1999; Cuenat and Aziz, 2002; Brown and Erlebacher, 2005; Brown et al., 2005), and also transient two-dimensional ripple

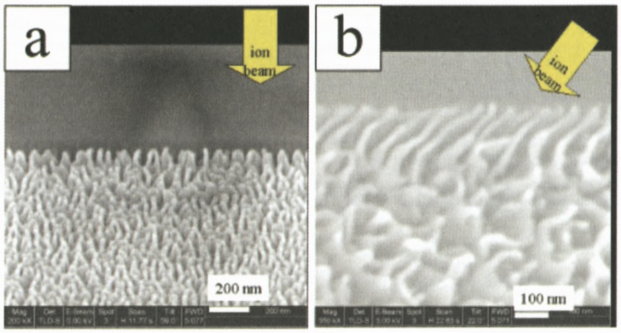

Figure 3. SEM image of Ge "nanograss" formed by uniform rastering with 30 keV Ga^+ FIB. (a) incident angle 90 degrees; (b) incident angle 60 degrees.

morphologies. For sputter patterns on Si, on which we will focus, the in-plane length scales (wavelengths) are typically of order 100 nm, and the out-of-plane length scales (amplitudes) are of order 10 nm. Spontaneously self-organized ripples and dots as small as 15 nm have been formed in other materials systems such as GaSb (Facsko et al., 2001) and SiO_2 (Mayer et al., 1994). We are studying the larger lateral length scales in Si because of the ready availability of *in-situ* probes, e.g. optical diffraction techniques (Chason et al., 1998; Erlebacher et al., 1999) and Focused Ion Beam (FIB)-Scanning Electron Microscopy (SEM) (Zhou et al., 2003) and because Si is a monatomic system highly amenable to atomistic modeling. With measurements at these length scales, we hope to rapidly develop a deep understanding of the fundamental aspects of the phenomenon. Ultimately we expect to develop sufficient understanding to design and guide experiments at sub-lithographic length scales that permits us to answer the question, "How much morphology control can one attain without having to write each individual feature?"

A significant recent discovery (Cuenat and Aziz, 2002; Habenicht et al., 2002) has been sputter patterning under uniform rastering of a focused ion beam (FIB), which is a machine typically used to micromachine surfaces in computer-controlled patterns. The rapid feedback possible with *in-situ* real-space imaging in a FIB instrument has accelerated the understanding of the phenomena believed to be common to both focused and unfocused ion irradiation. Not only has this observation of pattern evolution under FIB irradiation served as an excellent test of theory and motivated new theory, it has also lead to unanticipated developments, such as germanium "nanograss" shown in Figure 3 (Cuenat and Aziz, 2002).

2.2. Guided Self-Organization by Templating

Methods for the fabrication of large areas of nanoscale features with controlled period and intra-period organization are of interest because of the potential for high-throughput mass production of nanoscale devices. Due to their potential in this regard, much recent attention has been devoted to self-organization processes (Teichert et al., 1996; Facsko et al., 1999; Shchukin and Bimberg, 1999; Thurn-Albrecht et al., 2000). Although the short-range order can be quite high, some envisaged applications require long-range order, which is destroyed by uncontrolled topological defects arising spontaneously from the self-organization process. A potentially successful hierarchical fabrication strategy is the fabrication of controlled features at a small, but lithographically tractable, length scale by methods such as conventional mask or optical standing wave lithography, in order to guide a self-organization process at the finest length scale (Peters et al., 2000; Cheng et al., 2004). Lithographically- and Focused Ion Beam (FIB)-patterned topographies have recently been used to template quantum dot growth in linear chains (Yang et al., 2004), periodic 2D lattices (Karmous et al., 2004), and in more complex configurations promising for novel nanoelectronics architectures such as quantum cellular automata (Gray et al., 2004). The finest features have been templated by serial writing with the FIB, a prohibitively expensive process for mass production that might be circumvented by the hierarchical fabrication strategy. Self-organized sputter-ripple topographies have been used to template metal islands (Brown, 2005) and colloidal particles (Mathur et al., 2005) in linear chains.

We measured the influence of patterned boundaries on a Si(001) substrate in guiding self-organized sputter ripples (Cuenat et al., 2005). We showed that the long-range order of the features can be greatly enhanced by this lateral templating approach (Figure 4). The emerging pattern can be manipulated by changing the boundary spacing and misorientation with respect to the projected ion beam direction. We developed a scalar figure of merit, a dimensionless topological defect density, to characterize the degree of order of the pattern. At small boundary separation, the greatest order is observed when the separation is near an integer multiple of the spontaneously arising feature size. The defect density is exceedingly low up to a critical misorientation angle, beyond which topological defects develop in proportion to the incremental misorientation. No theory has been shown to predict the lateral templating effect and the documented behavior of the defect density, or to address the maximum distance between template boundaries over which it is possible to deterministically set the pattern that evolves within the intervening area. These remain open questions.

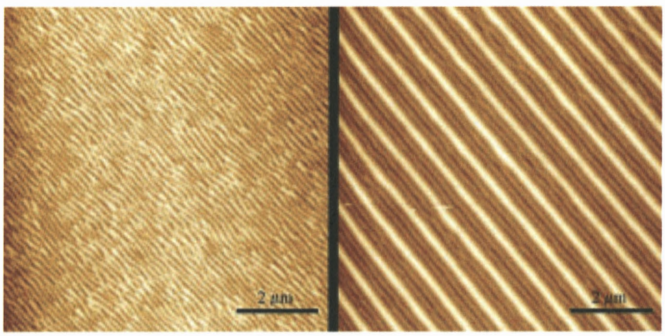

Figure 4. Lateral templating under ion beam sputtering (Cuenat et al., 2005). AFM topographs of sputter-rippled Si(001) just outside (left) and inside (right) lithographically templated region of same sample. High regions are white.

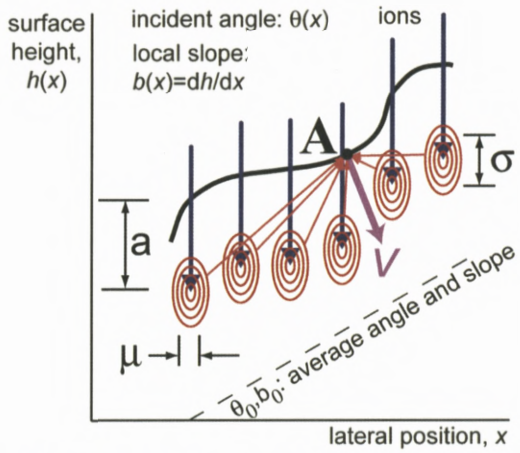

Figure 5. Sigmund's (1973) model of sputter morphology evolution. Iso-energy contours are illustrated. Average ion range is a, longitudinal and transverse straggling are σ and μ. As illustrated by red arrows, some energy from ions impinging at all points contributes to erosion at point **A**. Concave regions such as **A** are closer to the energy deposition maxima than convex regions and thereby erode faster.

2.3. Theory of Sputter Pattern Formation

All theories of sputter pattern formation originate from Sigmund's (1973) model demonstrating the instability of a planar surface to uniform ion beam erosion. Although treatments in two independent spatial dimensions are common, for the purpose of simplicity we will restrict our exposition to a single independent spatial dimension. As shown in Figure 5, let the ion beam approach the solid in the y

direction and let surface height be described by the function $y = h(x, t)$, where t is time. The rate of recession of an eroding surface (excluding surface relaxation and noise) can be written as $\partial h/\partial t = -V\sqrt{1 + b^2}$, where $b \equiv \partial h/\partial x$ is the local slope of the surface and V is the erosion speed normal to the surface. Generally, V is a function of the surface slope, curvature, and higher order derivatives of the morphology. According to Sigmund, V at point **A** at position **x** on the surface is proportional to the energy $E(x, x')$ deposited per unit depth at **x** from the collision cascades originating from ions impinging on the surface at all other points **x**′, as shown in Figure 5. The speed of erosion at **x** is then given by an integral over all points **x**′:

$$V(x) \propto \int \mathrm{d}x' E(x, x'). \tag{1}$$

As can be seen from Figure 5, concave regions of the surface, such as point **A**, are closer to the energy deposition maxima than convex regions and so erode faster. For simplicity, Sigmund modeled the distribution of deposited energy as centered a distance a below the impingement site (along the initial ion direction) and decaying outward as a Gaussian with an ellipsoidal shape. $E(x, x')$ then becomes simply

$$E(x, x') = \text{const.} \cdot \exp\left(-\frac{[h(h') - a - h(x)]^2}{2\sigma^2} - \frac{[x' - x]^2}{2\mu^2}\right). \tag{2}$$

We shall refer to the r.h.s. of Equation (1) as the *Sigmund sputter integral* and Equation (2) as the *Sigmund kernel*. Note that the only materials parameters controlling morphology evolution in this model are a, σ, and μ: parameters such as the surface binding energy merely scale the rates for all points on the surface by a multiplicative factor through the proportionality sign in Equation (1).

2.3.1. *Linear Stability Theory*

Bradley and Harper (BH) (1988) performed a linear stability analysis of a flat surface undergoing erosion according to the Sigmund kernel while simultaneously undergoing surface relaxation toward flatness by surface diffusion. They showed that the instability survives no matter how much relaxation by surface diffusion is occurring simultaneously. By expanding the height function for small curvature, slope difference, and height difference from a planar surface, they found that the leading order instability arises from the curvature coefficient of the sputter yield. The same expansion for the diffusional relaxation term is taken from the classical Mullins–Herring (Herring, 1950; Mullins, 1959) theory of morphological relaxation kinetics: The chemical potential is proportional to the surface tension

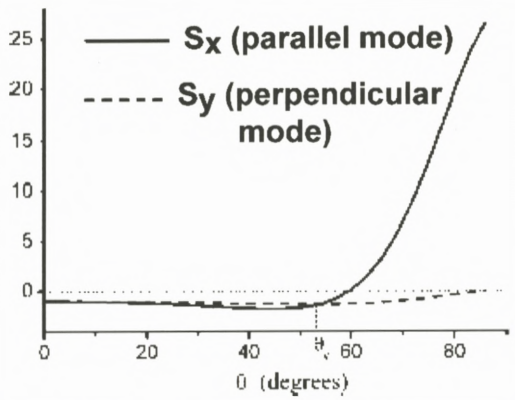

Figure 6. Variation of the curvature coefficient S of the vertical erosion rate (arbitrary units) in Equation (3) with inclination angle. Linear instability ($S < 0$) exists at all angles. When surface diffusion is isotropic, mode with most negative value of S is expected to dominate topography. Adapted from Feix et al. (2005).

times $\partial^2 h/\partial x^2$; the gradient of the chemical potential ($\sim\partial^3 h/\partial x^3$) determines the surface diffusion flux; and the divergence of the flux ($\sim\partial^4 h/\partial x^4$) gives the rate of change of height. The resulting partial differential equation (PDE) of BH for the change in height, relative to the average height, is

$$\frac{\partial h(x,t)}{\partial t} = S\frac{\partial^2 h}{\partial x^2} - B\frac{\partial^4 h}{\partial x^4}, \tag{3}$$

where the curvature coefficient S is negative, leading to instability. As a linear PDE, Equation (3) can be solved using Fourier methods. The amplitude of each Fourier component of the surface morphology $h_q(t)$ with wavenumber q should grow or decay exponentially with rate constant $R(q) = -Sq^2 - Bq^4$. BH thus predict a maximal value of $R(q)$ at a fastest growing spatial frequency $q^* = (-S/2B)^{1/2}$, so after a while the surface should be dominated by sinusoidal ripples with spatial period $\lambda^* = 2\pi/q^2$.

In two independent spatial dimensions, Bradley and Harper solved for the stability with respect to sinusoidal perturbations with wavevector either parallel or perpendicular to the direction of the projected ion beam on the surface ("parallel mode" and "perpendicular mode", respectively, Figure 2). As shown in Figure 6, all surfaces, at all angles of inclination θ, are predicted to be linearly unstable to perpendicular mode ripples, whereas all surfaces below a certain inclination angle (measured from normal) are predicted to be unstable to parallel mode ripples. Where instabilities to both modes arise, the resulting topography is expected to be

dominated by the mode with the greatest value of R. When surface diffusion is isotropic, this would be the mode with the most negative value of S.

The BH model also predicts the dependence of q^* and $R(q)$ on control parameters such as flux f and temperature T, and predicts that as long as the curvature and range of slope remain sufficiently small, the fastest growing spatial period should be time-independent. The model has been tested under a wide variety of conditions and has been found to describe some aspects of evolution but not others Chason, in these proceedings, describes tests of BH for copper surfaces under a wide range of conditions. For silicon, the flux-dependence and temperature-dependence of λ^* is consistent with BH (Erlebacher et al., 1999); λ^* is time-independent for Si(001) (Erlebacher et al., 1999, 2000b) but, contrary to BH, coarsens with time for Si(111) (Brown and Erlebacher, 2005). One commonly observes amplitude saturation at long times, which one expects would arise from nonlinear terms missing from a linear stability theory, but in silicon saturation is occurring at surprisingly small slopes ($\sim 10°$) that are difficult to understand (Erlebacher et al., 2000b; Brown and Erlebacher, 2005). Transient topographies not predicted by BH are observed on Si(111) (Brown et al., 2005).

One common example of the curious failure of BH theory is for normal-incidence unfocused ion irradiation, where an instability with a characteristic length scale is predicted but rarely observed (Cuenat and Aziz, 2002) (with a few notable exceptions, e.g. Facsko et al., 2001). Beyond this, the experimental conditions for stability are not clear. We now have evidence that under certain conditions the sputter instability is actually a sputter metastability, i.e., an initially flat, amorphous surface is metastable.

Because the BH linear stability results are a rigorous consequence of formulae (1, 2), one must examine the validity of the Sigmund theory underlying just about every treatment of morphological development. Recently Feix et al. (2005) reported molecular dynamics simulations of the sputter erosion of copper crystals by 5 keV Cu. They looked at the spatial distribution of sites from which the sputtered atoms were emitted with respect to the point of impact and found that Equation (1) describes their results pretty well (assuming V is proportional to the atom emission rate, which they tracked), except that the Sigmund kernel, Equation (2), needed to be replaced by a kernel of a somewhat different form. This permitted them to explain a reduction in sputter yield with increasing angle at very high angles, which is not explained by the Gaussian ellipsoid kernel (see Figure 10), but otherwise the results of the Sigmund model seem to be qualitatively unchanged. In particular, with a modified sputter kernel of Feix et al., the qualitative features of Figure 6 remain the same: all surfaces at all inclinations *should* exhibit a linear instability.

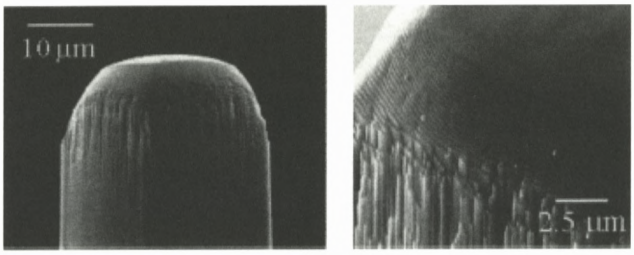

Figure 7. Example of tall, steep features that cannot be modeled with a perturbative approach. Single crystal diamond curved tip microindenter fabricated by FIB, from Adams et al. (2003). High-magnification view on the right shows three different morphologies, including rippled "phase" and flat "phase".

We have accumulated reasons to believe that other forms of the sputter kernel qualitatively change the conclusions on stability. Other kernels may result from a variety of effects. For example, under some conditions, ion impacts create craters with rims (Bringa et al., 2001). In all cases, the ion-induced change in topography $\Delta h(x - x')$ can be characterized quantitatively (Moseler et al., 2005). Because of effects such as thermal spikes or ion-stimulated mass transport at or near the surface, V is *not* necessarily proportional to the atom emission rate. We are working on understanding the consequences when the Sigmund kernel is replaced in Equation (1) by an expression for the local topography change (Kalyanasundaram et al., unpublished), resulting in

$$\frac{\partial h(x,t)}{\partial t} = \int J(x')\Delta h(x, x'; b)\, \mathrm{d}x', \tag{4}$$

where J is the ion flux and b is the local slope. Our conjecture is that this will create a term $S'\partial^2 h/\partial x^2$ that can overwhelm the first term on the r.h.s. of Equation (3), thereby becoming the predominant source of linear stability or instability.

2.3.2. *Nonlinear Perturbative Approach*

Enhancements to BH theory have been made to include noise (Mayer et al., 1994), nonlinear effects at larger amplitudes (Park et al., 1999; Makeev et al., 2002; Castro et al., 2005), and the identification (Makeev and Barabasi, 1997) of a fourth-order "effective surface diffusion" term $-D_{xx}\partial^4 h/\partial x^4$ through which we can understand how patterns may form even when surface diffusion is essentially turned off at low temperature where $B = 0$.

The inclusion of nonlinear effects is an area of very active research. Makeev and co-workers (Makeev et al., 2002) developed from the Sigmund kernel a general expression for V in terms of arbitrary topography and the parameters a, σ,

and μ describing the ion collision cascade in the solid. To obtain solutions, they then expanded V in powers of slope and derived an erosion equation of the form (for simplicity we report only the most noteworthy terms in a one-dimensional version although the actual theory is for two independent spatial dimensions)

$$\frac{\partial h}{\partial t} = S_x \left(\frac{\partial^2 h}{\partial x^2}\right) + \xi_x \left(\frac{\partial h}{\partial x}\right)\left(\frac{\partial^2 h}{\partial x^2}\right) + \Omega_1 \frac{\partial^3 h}{\partial x^3} - D_{xx}\frac{\partial^4 h}{\partial x^4} + \frac{\lambda_x}{2}\left(\frac{\partial h}{\partial x}\right)^2, \quad (5)$$

where S_x, x_x, and W_1 are roughening prefactors determining the anisotropic erosion rate, D_{xx} describes ion induced "effective surface diffusion", and λ_x controls the early stages of nonlinear evolution. Makeev et al. solved for these ion-related coefficients as functions a, σ, and μ. Solutions to the two-dimensional counterpart of Equation (5) have been obtained for shallow ripples (Makeev et al., 2002; Makeev and Barabasi, 2004b) and self-affine surfaces (Makeev and Barabasi, 2004a).

Makeev et al.'s small-slope expansion, Equation (5), is valid for slope excursions of several tens of degrees, but cannot be used to describe our observed lateral templating of sputter ripples (Figure 4) because experimentally the initial surface possesses regions of widely differing slopes. Likewise, understanding and controlling the effects of the FIB on morphology evolution in the micromachining of tall, steep features remains open (Vasile et al., 1999; Adams et al., 2003; Tseng et al., 2004). What we need in cases such as these is a non-perturbative approach that can handle arbitrarily large excursions in inclination angle

2.3.3. *Erosion of Tall, Steep Features*

We have reported a new regime of ion beam sputtering that occurs for sufficiently steep slopes (Chen et al., 2005). High slopes propagate over large distances without dissipating the steepest features. Both the propagation velocity and the dynamically selected slope are universal, independent of the details of the initial shape of the surface. The SEM image in Figure 8 shows a pit with steep side walls that has been micromachined into silicon using a Focused Ion Beam, and to the right the same pit, with sides that have not smeared out, after uniform ion irradiation of the entire wafer. The left panel of Figure 9 shows predictions of the new theory of sputter morphology evolution that is valid for arbitrarily large slopes when the curvature is small. Under uniform ion irradiation the pit wall, initially at $t = 0$, propagates laterally and, for this particular set of conditions, evolves to maintain a uniform slope that is steeper than the original slope. The theory also predicts that sufficiently shallow slopes dissipate, which is the conventionally observed behavior. The experimental sequence in Figure 9, obtained with an optical profilometer, shows striking confirmation of the predictions of the

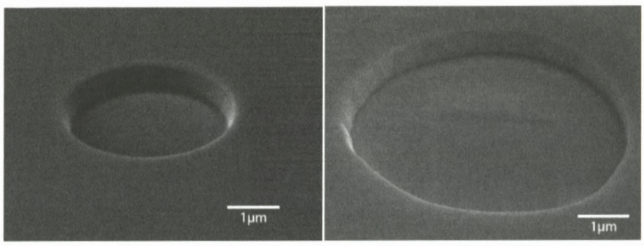

Figure 8. (a) SEM image of an initial circular pit in Si with 3 μm diameter, 0.5 μm depth, and steep side walls. (b) The wall of the enlarged pit is still sharp after uniform ion exposure. From Chen et al. (2005).

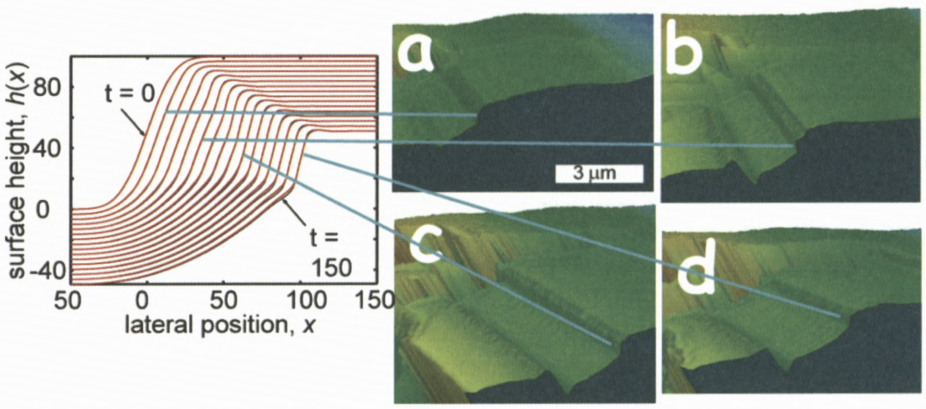

Figure 9. (Left) Theoretical profile evolution. Red curves: solution of advection-diffusion PDE; black curves: numerical integration of Sigmund kernel. (a)–(d) Experimental profiles illustrating propagation of shock front with decreasing height and increasing size of trailing rarefaction wave. The blue lines are for illustrative purposes and do not signify a quantitative one-to-one correspondence between theoretical and experimental profiles. Adapted from Chen et al. (2005).

theory. An important implication of the transition from dissipative behavior to propagative behavior at high slopes is that a structure (e.g. line or dot) can be fabricated at a large length scale and, with uniform ion irradiation, reduced to a smaller length scale while preserving, or even sharpening, the steepest features.

The non-perturbative approach for steep features develops from the Sigmund sputter kernel a small-curvature approximation that is valid for *all* slopes. Combining this with Mullins–Herring surface diffusion mediated surface smoothening results in a nonlinear PDE called the advection-diffusion equation,

$$\frac{\partial b(x,t)}{\partial t} = -C\frac{\partial b}{\partial x} - S\frac{\partial^2 b}{\partial x^2} - B\frac{\partial^4 b}{\partial x^4}, \tag{6}$$

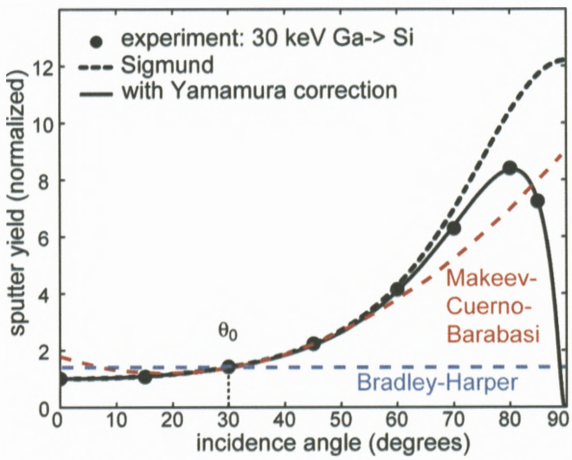

Figure 10. Sputter yield of flat surface *versus* incidence angle. Adapted from Vasile et al. (1999). Dashed curve: full Sigmund sputter integral with Sigmund kernel(Gaussian ellipsoids). Solid black: with empirical Yamamura correction (Yamamura et al., 1983; Vasile et al., 1999). Applying Bradley–Harper analysis to large amplitudes assumes all coefficients are constant at their initial value, e.g. illustrated here for an initial slope of 30°. Red curve: Makeev et al.'s quadratic expansion in powers of slope. The entire black curve goes into the non-perturbative theory of Chen et al.; shock fronts result in the region where the curvature is downward.

where $b \equiv \partial h/\partial x$ b is the slope, $C = C(b) \equiv \partial Y/\partial b$ turns out to be the propagation speed, and Y is the sputter yield (see Figure 10). The solutions of this equation predict behavior that can be understood as the propagation of a shock front that self-selects a stable slope; the mathematical structure of the solutions is the same as that previously observed in thin-film fluid flows. The shock front behavior turns out to be a generic feature of the non-monotonic behavior of the sputter yield *versus* slope. As the slope increases, the center of the energy deposition gets closer to the surface; hence the sputter yield increases with slope. But at high enough slope, the sputter yield turns down again due to effects such as reflection at grazing incidence (Yamamura et al., 1983) and incomplete development of the collision cascade (Sigmund, 1981), and possibly to deviations of the true collision cascade shape from Gaussian ellipsoids (Feix et al., 2005). This qualitative behavior of the sputter yield *versus* slope, combined with the kinetics of surface diffusion, turns out to be sufficient for propagative rather than dissipative solutions to the morphology evolution equation arising from the Sigmund sputter kernel and fourth-order diffusion.

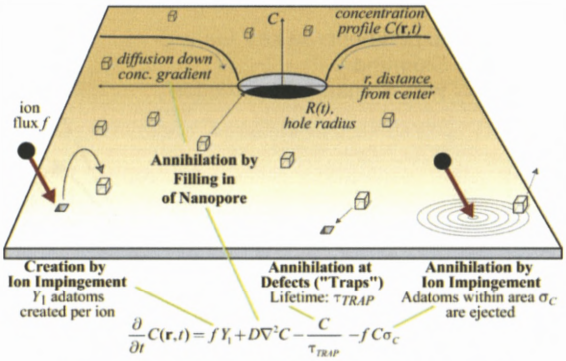

Figure 11. Processes in adatom diffusion model.

3. Single Biomolecule Detectors

The physics and materials science of sputter patterning are important in the development of nanopore single- molecule detectors (Figure 12). Focused and unfocused ion beam irradiation has been used to fabricate single nanopores in insulators, control their diameters to molecular dimensions, and use them in sensitive devices to detect and analyze single biomolecules in solution (Li et al., 2001, 2003; Stein et al., 2002, 2004; Chen et al., 2004; Mitsui et al., 2006) Such detectors are envisaged as DNA sequencers $\sim 10^6$ times faster than those in current use (Meller et al., 2000). Using a FIB of 50 keV Ga^+, single nanopores of diameter $\sim$ 50 nm are drilled through a membrane of silicon dioxide or silicon nitride supported along its perimeter by attachment to a silicon wafer substrate. Subsequent broad irradiation with an unfocused beam of 3 keV Ar^+ results in the gradual closure of the nanopore. Feedback on the transmitted ion current permits an exquisite level of control on the final pore diameter, which can be tuned to pass molecules with diameters under a desired value. An adatom-diffusion model (Figure 11), which is an extension of the model of the atomistic processes occurring in sputter patterning of Si(001) (Erlebacher et al., 1999), accounts for many aspects of the ion-sputter-induced closing of nanopores in silicon nitride membranes (Li et al., 2001) (Figure 12). This model posits that the spatiotemporal evolution of the concentration field $C(\mathbf{r}, t)$ of surface-diffusing mobile species ("adatoms") created by the ion beam is governed by the following PDE:

$$\frac{\partial}{\partial t}C(\mathbf{r}, t) = fY_1 - \frac{C}{\tau_{\text{trap}}} - fC\sigma + D\nabla^2 C, \tag{7}$$

where f is the ion flux, Y_1 is the number of adatoms created per incident ion, τ_{trap} is a time constant for annihilation by fixed traps, σ is the cross section for adatom

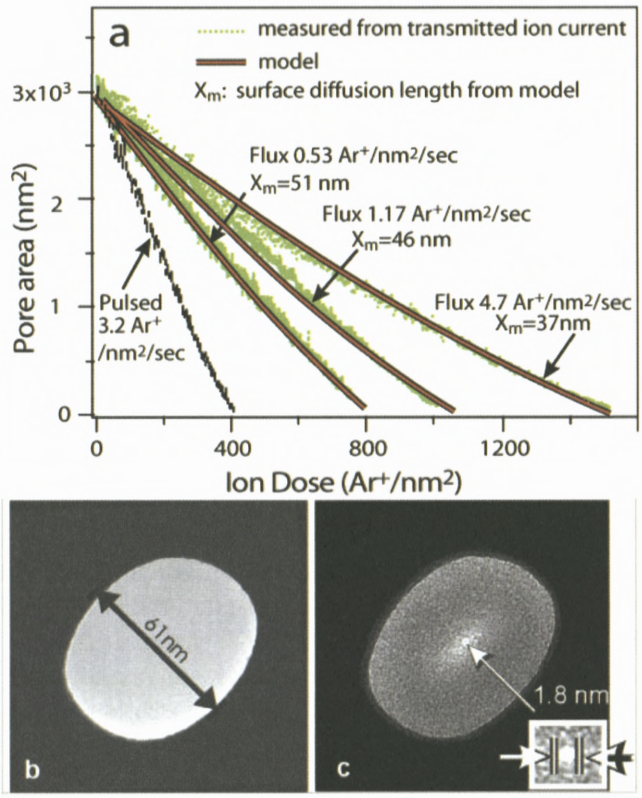

Figure 12. (a) Pore area determined by ion beam current transmitted through nanopore *versus* dose. (b) TEM image of initial ~ 60 nm pore in a 500 nm thick Si_3N_4 membrane made by focused ion beam. (c) TEM image of sample after subsequent unfocused 3 keV Ar^+ ion irradiation during which pore fills with electron transparent (~ 10 nm thick) membrane; final diameter 1.8 nm. Adapted from Li et al. (2001).

annihilation by direct ion impingement, and D is the adatom diffusivity. Adatoms that diffuse to the edge of the pore fill it in; the diffusional flux to the edge of the pore is determined by the concentration gradient at the edge of the pore in the steady-state solution to Equation (7). This flux then determines the closing rate of the pore, which is given by

$$\frac{\mathrm{d}}{\mathrm{d}t}(\pi R^2) = \frac{2\pi R\Omega f}{H}\left(Y_p - Y_a X_m \frac{K_1(R/X_m)}{K_0(R/X_m)}\right), \tag{8}$$

where R is the pore radius, Ω is the adatom volume, H is the pore thickness, Y_p is the opening contribution from ion beam sputter erosion of the edge of

the pore, Y_a is the adatom yield, X_m is the average surface diffusion length of adatoms before annihilation by fixed traps or ion impingement, and K_0 and K_1 are Bessel functions that arise from the solution to the diffusion equation in polar coordinates.

The model successfully accounts for several observations including (a) the measured time-dependence of the nanopore area during irradiation; (b) the decreased effectiveness of nanopore closing, per ion, at higher fluxes due to increased beam-induced "adatom" annihilation; (c) the increased effectiveness of nanopore closing, per ion, if the same flux is delivered in pulses separated by "offtime", to the same total fluence; (d) the strong temperature-dependence of the closing rate; (e) the existence of a maximum size pore that can be closed under ion exposure. Representative results are shown in Figure 12(a).

Although nanopores close in SiO_2 (Stein et al., 2002), the material appears to respond differently than silicon nitride, e.g. the rate is rather insensitive to temperature. We are considering the possibility that ion stimulated viscous flow (Snoeks et al., 1995; Umbach et al., 2001), possibly in conjunction with ion-stimulated compressive stress (Brongersma et al., 2000; van Dillen et al., 2005), mediates morphology evolution in this system. Electrostatic effects and ionic conduction during irradiation also appear to be important (Mitsui et al., 2006).

We anticipate that different classes of materials may be found in which different mechanisms mediate transport. For example, surface-confined viscous flow via an ion-enhanced fluidity has been identified as the transport mechanism in sputter rippling of SiO_2 with keV ion beams (Mayer et al., 1994; Umbach et al., 2001). The nanopore-closing results on amorphous silicon nitride are quantitatively consistent with the adatom diffusion model and qualitatively inconsistent with at least one key aspect of the ion-enhanced fluidity mechanism, namely the observed dependence of closure-per-ion on flux and on offtime between ion pulses: in current models for ion-enhanced fluidity, only the ion fluence matters and not its temporal dependence. Results in SiO_2 are also qualitatively inconsistent with this same key aspect of the ion-enhanced fluidity mechanism in its current form (Stein et al., 2002). It is more difficult to envisage viscous flow as an important mechanism in materials that remain crystalline under ion irradiation, in either single-crystal or large-grain polycrystal form, as metals do at typical temperatures and Si and Ge do at sufficiently high temperature.

4. Surface Morphological Relaxation and Nanostructure Stability

Much recent research has been focused on a better understanding of the sputter yield and its nonlinear dependence on elements of the surface topography.

However, all analytical treatments of morphology evolution under ion erosion generally assume surface diffusion mediated smoothening governed by the final term in Equation (3), $B\partial^4 h/\partial x^4$, where B contains the surface diffusion coefficient. This classical Mullins–Herring term is known to be valid for amorphous solids and crystalline surfaces above the thermodynamic roughening transition temperature. However, we have shown that under thermal annealing conditions after the ion beam is turned off, sputter patterned Si(001) surfaces obey non-classical relaxation kinetics inconsistent with $B\partial^4 h/\partial x^4$ (Erlebacher et al., 2000a; Pedemonte et al., 2003). As are most crystalline surfaces under typical materials processing conditions, these surfaces are well below their roughening transition temperature. Non-classical effects appear to be responsible for the change of the decay kinetics of the corrugation amplitude $A(t)$ from exponential decay to inverse linear,

$$A(t) = \frac{A(0)}{1 + kt}, \tag{9}$$

where k is a wavelength and temperature dependent rate constant. An important element of a non-classical approach leading to inverse linear decay under the observed conditions appears to be a description of the surface as a collection of atomic steps separated by flat terraces (Israeli and Kandel, 2000; Margetis et al., 2005; Margetis, 2006). It remains an open question whether a crystalline surface below its thermodynamic roughening transition temperature can be driven by ion beam irradiation into a dynamically roughened state for which the classical description remains valid.

Acknowledgements

I am indebted to my students, postdocs and collaborators, whose contributions have been critical to the understanding of many of the phenomena discussed here: Jack Blakely, Dan Branton, Michael Brenner, Ari Brown, Kee-Chul Chang, Eric Chason, Henry Chen, Alexandre Cuenat, Benny Davidovitch, Jonah Erlebacher, Jerry Floro, Jonathan Freund, H. Bola George, Jene Golovchenko, Stefan Ichim, Harley Johnson, Nagarajan Kalyanasundaram, Jiali Li, Dionisios Margetis, Ciaran McMullan, Humberto Rodriguez, Mike Sinclair, Derek Stein, Howard Stone, Omar Urquidez, and Wei Zhou. This research was supported initially by U.S. Department of Energy grant DE-FG02-01ER45947 and subsequently by U.S. National Science Foundation grant DMR-0306997.

References

Adams D.P., Vasile M.J., Mayer T.M. and Hodges V.C. (2003): Focused ion beam milling of diamond: Effects of H_2O on yield, surface morphology and microstructure. J Vac Sci Technol B **21**, 2334–2343

Bradley R.M. and Harper J.M. (1988): Theory of ripple topography induced by ion bombardment. J Vac Sci Technol A **6**, 2390

Bringa E.M., Nordlund K. and Keinonen J. (2001): Cratering-energy regimes: From linear collision cascades to heat spikes to macroscopic impacts. Phys Rev B **64**, 235426–235437

Brongersma M.L., Snoeks E., van Dillen T. and Polman A. (2000): Origin of MeV ion irradiation-induced stress changes in SiO_2. J Appl Phys **88**, 59–64

Brown A.D. (2005). Studies of ion sputtered Si(111) surfaces. Ph.D. Thesis, Johns Hopkins University, Baltimore, MD

Brown A.D. and Erlebacher J. (2005): Temperature and fluence effects on the evolution of regular surface morphologies on ion-sputtered Si(111). Phys Rev B **72**, 075350

Brown A.D., Erlebacher J., Chan W.L. and Chason E. (2005): Transient topographies of ion patterned Si(111). Phys Rev Lett **95**, 056101

Castro M., Cuerno R., Vazquez L. and Gago R. (2005): Self-organized ordering of nanostructures produced by ion-beam sputtering. Phys Rev Lett **94**, 016102

Chason E., Sinclair M.B., Floro J.A., Hunter J.A. and Hwang R.Q. (1998): Spectroscopic light scattering for real- time measurements of thin film and surface evolution. Appl Phys Lett **72**, 3276

Chen H.H., Urquidez O.A., Ichim S., Rodriguez L.H., Brenner M.P. and Aziz M.J. (2005): Shocks in ion sputtering sharpen steep surface features. Science **310**, 294–297

Chen P., Gu J.J., Brandin E., Kim Y.R., Wang Q. and Branton D. (2004): Probing single DNA molecule transport using fabricated nanopores. Nano Lett **4** 2293–2298

Cheng J.Y., Mayes A.M. and Ross C.A. (2004): Nanostructure engineering by templated self-assembly of block copolymers. Nature Materials **3**, 823–828

Cuenat A. and Aziz M.J. (2002): Spontaneous pattern formation from focused and unfocused ion beam irradiation. Mater Res Soc Symp Proc **696**, N2.8.1

Cuenat A., George H.B., Chang K.C., Blakely J. and Aziz M.J. (2005): Lateral templating for guided self-organization of sputter morphologies. Advanced Materials **17**, 2845–2849

Erlebacher J.D. and Aziz M.J. (1997): Ion-sputter induced rippling of Si(111). Mater Res Soc Symp Proc **440**, 461–466

Erlebacher J., Aziz M., Chason E., Sinclair M. and Floro J. (1999): Spontaneous pattern formation on ion bombarded Si(001). Phys Rev Lett **82**, 2330–2333

Erlebacher J., Aziz M.J., Chason E., Sinclair M.B. and Floro J.A. (2000a): Nonclassical smoothening of nanoscale surface corrugations. Phys Rev Lett **84**, 5800–5803

Erlebacher J., Aziz M.J., Chason E., Sinclair M.B. and Floro J.A. (2000b): Nonlinear amplitude evolution during spontaneous patterning of ion-bombarded Si(001). J Vacuum Sci Technol A **18**, 115–120

Facsko S., Dekorsy T., Koerdt C., Trappe C., Kurz H., Vogt A. and Hartnagel H.L. (1999): Formation of ordered nanoscale semiconductor dots by ion sputtering. Science **285**, 1551–1553

Facsko S., Bobek T., Dekorsy T. and Kurz H. (2001): Ordered quantum dot formation by ion sputtering. Phys Stat Sol B **224**, 537–540

Feix M., Hartmann A.K., Kree R., Munoz-Garcia J. and Cuerno R. (2005): Influence of collision cascade statistics on pattern formation of ion-sputtered surfaces. Phys Rev B **71**, 125407

Gray J.L., Atha S., Hull R. and Floro J.A. (2004): Hierarchical self-assembly of epitaxial semiconductor nanostructures. Nano Lett **4** 2447–2450

Habenicht S. (2001): The morphology of graphite surfaces after ion beam erosion. Phys Rev B **63**, 125419

Habenicht S., Lieb K.P., Koch J. and Wieck A.D. (2002): Ripple propagation and velocity dispersion on ion-beam-eroded silicon surfaces. Phys Rev B **65**, 115327

Herring C. (1950): Effect of change of scale on sintering phenomena. J Appl Phys **21**, 301–303

Israeli N. and Kandel D. (2000): Decay of one-dimensional surface modulations. Phys Rev B **62**, 13707–13717

Kalyanasundaram N., Davidovitch B., Johnson H.T., Freund J.B., Brenner M.P. and Aziz M.J. (unpublished).

Karmous A., Cuenat A., Ronda A., Berbezier I., Atha S. and Hull R. (2004): Ge dot organization on Si substrates patterned by focused ion beam. Appl Phys Lett **85**, 6401–6403

Li J., Stein D., McMullan C., Branton D., Aziz M.J. and Golovchenko J. (2001): Ion beam sculpting at nanometre length scales. Nature **412**, 166–169

Li J., Gershow M., Stein D., Brandin E. and Golovchenko J.A. (2003): DNA molecules and configurations in a solid state nanopore microscope. Nature Materials **2**, 611–615

Makeev M.A. and Barabasi A.-L. (1997): Ion-induced effective surface diffusion in ion sputtering. Appl Phys Lett **71** 2800–2802

Makeev M.A. and Barabasi A.-L. (2004a): Effect of surface morphology on the sputtering yields. I. Ion sputtering from self-affine surfaces. Nucl Instrum Meth B **222**, 316–334

Makeev M.A. and Barabasi A.-L. (2004b): Effect of surface morphology on the sputtering yields. II. Ion sputtering from rippled surfaces. Nucl Instrum Meth B **222**, 335–354

Makeev M.A., Cuerno R. and Barabasi A.-L. (2002): Morphology of ion-sputtered surfaces. Nucl Instrum Meth B **197**, 185–227

Margetis D. (2006): Unified continuum approach to crystal surface morphological relaxation. Submitted

Margetis D., Aziz M.J. and Stone H.A. (2005): Continuum approach to self-similarity and scaling in nanostructure decay. Phys Rev B **71**, 165432

Mathur A., Brown A.D. and Erlebacher J. (2005): Self-ordering of colloidal particles in shallow nanoscale surface corrugations. Langmuir **22**, 582–589

Mayer T.M., Chason E. and Howard A.J. (1994): Roughening instability and ion-induced viscous relaxation of SiO_2 surfaces. J Appl Phys **76** 1633–1643

Meller A., Nivon L., Brandin E., Golovchenko J. and Branton D. (2000): Rapid nanopore discrimination between single polynucleotide molecules. Proc Nat Acad Sci USA **97**, 1079–1084

Mitsui T., Stein D., Kim Y.R., Hoogerheide D. and Golovchenko J.A. (2006): Nanoscale volcanoes: Accretion of matter at ion-sculpted nanopores. Phys Rev Lett **96**, 036102

Moseler M., Gumbsch P., Casiraghi C., Ferrari A.C. and Robertson J. (2005): The ultrasmoothness of diamond-like carbon surfaces. Science **309**, 1545–1549

Mullins W.W. (1959): Flattening of a nearly plane solid surface due to capillarity. J Appl Phys **30**, 77

Navez M., Chaperot D. and Sella C. (1962): Microscopie electronique – étude de lattaque du verre par bombardement ionique. C R Hebdomadaires Seances Acad Sci **254**, 240

Park S., Kahng B., Jeong H. and Barabasi A.-L. (1999): Dynamics of ripple formation in sputter erosion: Nonlinear phenomena. Phys Rev Lett **83**, 3486–3489

Pedemonte L., Bracco G., Boragno C., Mongeot F.B. and Valbusa U. (2003): Smoothing of nanoscale surface ripples studied by He atom scattering. Phys Rev B **68**, 115431

Peters R.D., Yang X.M., Wang Q., de Pablo J.J. and Nealey P.F. (2000): Combining advanced lithographic techniques and self-assembly of thin films of diblock copolymers to produce templates for nanofabrication. J Vac Sci Technol B **18**, 3530–3534

Shchukin V.A. and Bimberg D. (1999): Spontaneous ordering of nanostructures on crystal surfaces. Rev Mod Phys **71**, 1125–1171

Sigmund P. (1973): A mechanism of surface micro-roughening by ion bombardment. J Mater Sci **8**, 1545–1553

Sigmund P. (1981): Sputtering by ion bombardment: Theoretical concepts. In: Sputtering by Particle Bombardment I, Behrisch R. (Ed.), Springer-Verlag, Berlin, pp 9–71

Snoeks E., Weber T., Cacciato A. and Polman A. (1995): MeV ion irradiation-induced creation and relaxation of mechanical stress in silica. J Appl Phys **78**, 4723–4732

Stein D., Li J. and Golovchenko J.A. (2002): Ion beam sculpting time scales. Phys Rev Lett **89**, 276106

Stein D.M., McMullan C.J., Li J.L. and Golovchenko J.A. (2004): Feedback-controlled ion beam sculpting apparatus. Rev Sci Instrum **75**, 900–905

Teichert C., Lagally M.G., Peticolas L.J., Bean J.C. and Tersoff J. (1996): Stress-induced self-organization of nanoscale structures in SiGe/Si multilayer films. Phys Rev B **53**, 16334–16337

Thurn-Albrecht T., Schotter J., Kastle C.A., Emley N., Shibauchi T., Krusin-Elbaum L., Guarini K., Black C.T., Tuominen M.T. and Russell T.P. (2000): Ultrahigh-density nanowire arrays grown in self-assembled diblock copolymer templates. Science **290**, 2126–2129

Tseng A.A., Insua I.A., Park J.S., Li B. and Vakanas G.P. (2004): Milling of submicron channels on gold layer using double charged arsenic ion beam. J Vac Technol B **22**, 82–89

Umbach C.C., Headrick R.L. and Chang K.C. (2001): Spontaneous nanoscale corrugation of ion-eroded SiO2: The role of ion-irradiation-enhanced viscous flow. Phys Rev Lett **87**, 246104

Valbusa U., Boragno C. and de Mongeot F.B. (2003): Nanostructuring by ion beam. Mater Sci Engrg C **23**, 201–209

van Dillen T., Polman A., Onck P.R. and van der Giessen E. (2005): Anisotropic plastic deformation by viscous flow in ion tracks. Phys Rev B **71**, 024103

Vasile M.J., Xie J.S. and Nassar R. (1999): Depth control of focused ion-beam milling from a numerical model of the sputter process. J Vac Sci Technol B **17**, 3085–3090

Yamamura Y., Itikawa Y. and Itoh N. (1983): Angular dependence of sputtering yields of monatomic solids. Nagoya, Japan, Institute of Plasma Physics, Nagoya University

Yang B., Liu F. and Lagally M.G. (2004): Local strain-mediated chemical potential control of quantum dot self-organization in heteroepitaxy. Phys Rev Lett **92**, 025502

Zhou W., Cuenat A. and Aziz M.J. (2003): Formation of self-organized nanostructures on Ge during focused ion beam sputtering. In: Microscopy of Semiconducting Materials 2003: Proceedings of the 13th International Conference on Microscopy of Semiconducting Materials, Cullis A.G. and Midgley P.A. (Eds), IOP